RANJAN VEPA, KANELLA PETRAKOU
Queen Mary, University of London

INERTIAL NAVIGATION POSITION AND ORIENTATION ESTIMATION WITH OCCASIONAL GALILEO SATELLITE POSITION FIXES AND STEREO CAMERA MEASUREMENTS

ABSTRACT

In this paper an adaptive unscented Kalman filter based mixing filter is used to integrate kinematic satellite aided inertial navigation system with vision based measurements of five representative points on a runway in a modern receiver that incorporates carrier phase smoothing and ambiguity resolution. Using high resolution multiple stereo camera based measurements of five points on the runway, in addition to a set of typical pseudo-range estimates that can be obtained from a satellite navigation system such GPS or GNSS equipped with a carrier phase receiver, the feasibility of generating high precision estimates of the typical outputs from an inertial navigation system is demonstrated. The methodology may be developed as a stand-alone system or employed in conjunction with a traditional strapped down inertial navigation systems for purposes of initial alignment. Moreover the feasibility of employing adaptive mixing was explored as it facilitates the possibility of using the system for developing a vision based automatic landing controller.

Keywords:
vision-based navigation, inertial navigation system, Galileo, GNSS.

INTRODUCTION

Autonomous landing is a challenging and important task for both manned and unmanned vehicles if one wishes to achieve a high level of autonomy. The fundamental requirement for landing is the precise knowledge of the height and pose of the vehicle above the ground particularly in relation to the landing strip or runway. With a precise knowledge of the aircraft's height and pose and a properly designed controller to govern the landing process, autonomous landing of the vehicle can be

achieved safely and smoothly. One of the primary aids which can form the basis of an autonomous landing system is a satellite based navigation system which can provide precise estimates of the aircraft's position and orientation in space. However a vision sensor providing measurements of the landing strip or runway can substantially improve although not guarantee a safe and smooth landing. To guarantee a safe and smooth landing, complimentary measurements from several sensing systems including inertial, satellite and vision systems must be 'mixed' to provide a robust estimate of the vehicles position and orientation relative to the landing strip. Moreover, a vision system is the only sensor that can also provide runway recognition thus allowing the vehicle to autonomously decide on landing at a particular location.

Approach and landing are known to be the most demanding phases in a commercial flight. Due to the altitudes involved pilots must interpret position, attitude and distance to the runway using only two-dimensional cues like perspective, angular size and movement of the runway. At the same time, all six degrees-of-freedom of the aircraft must be estimated and controlled in order to meet and track the correct glide path and flare till touchdown. Image-based estimation of a typical landmark's spatial position and orientation provides useful information which can be used to correct the aircraft's position and orientation in real time. In particular, during landing the landmark in question could be the geometry of specific runways as seen from the camera attached to an aircraft in flight. The runway geometry is assumed to be fully known in space fixed coordinates. Thus by measuring key intersection points on the runway and given the spatial position of these points in a fixed reference frame, one would be able to obtain accurate updates of an aircraft's navigation position and orientation obtained a satellite navigation system such as GPS or GNSS.

The focus of recent research for estimating the attitude and position of a vehicle from Line-of-Sight (LOS), or bearing, measurements of a known landmark has been in the area of vision or camera based measurements. Typically a Kalman filter or one of a variety of extended Kalman filters (EKF) is used to estimate the relative position and orientation of the vehicle relative to the landmark. The filter fuses measurements from an Inertial Navigation System (INS) with camera based measurements using an optical sensor incorporating a position-sensing diode (PSD) to detect custom light beacons in the landmark. One such system is the Vision based Navigation system (VISNAV) which uses a PSD embedded within the camera's image plane rather than the traditional Charge Coupled Device (CCD) based camera. While a CCD is an array of closely spaced MOS diodes that detect the peak value of the light distribution over an active area for each pixel and give a sequential digital output, PSDs are purely analog devices that generate a current in a photodiode and divide it in one

or two resistive layers thereby measuring the position of the centre of gravity of a light spot. Thus a VISNAV type sensor can provide multiple line-of-sight vectors from an aircraft to a runway, provided the runway is fitted with appropriate light beacons along its boundaries. Consequently a VISNAV type system facilitates the simultaneous estimation of both relative position and attitude.

Simultaneous Localization and Mapping (SLAM) methods constitute a family of approaches for mixing inertial measurements with camera based observations [11, 12, 24]. Several algorithms have been developed for SLAM applications which jointly estimate the camera pose and the 3D feature positions, thus eliminating the need for a pre-loaded map. The performance of SLAM for aircraft landing applications is dependent on the nature of mapped landmarks (such as runway borders or runway centre-line) that are detected to estimate the camera's absolute pose. There have been a limited number of studies, [17, 22, 26], of the feasibility of mixing vision based measurements with inertial navigation systems for aircraft navigation applications. The presence of well defined and pre-mapped landmarks makes the system state observable thus eliminating the undesirable effects of partial observability [1]. A mapped landmark-aided localization approach using vision, inertial and satellite navigation sensors (such as GPS, GLONASS or the emerging European GNSS systems) has several advantages because information from a range of diverse sensors is being combined to generate an accurate estimate of the aircraft's orientation and position coordinates. The advantages stem from the fact that the measurements from these systems are complimentary.

Integration of inertial navigation systems (INS), satellite navigation systems (SNS) and vision sensors (VS) can be classified based on the extent to which the measurements from each of the systems are shared, either by the component sub-systems or by a centralised processor seeking to combine them. When the data is provided to each individual component sub-system to improve its performance via feedback or feed forward connections while retaining the independent processing ability of each component sub-system, the overall integrated system is said to be loosely coupled. For example GPS derived estimates of the aircraft's position could be provided to an inertial measuring unit (IMU) to update its outputs continually. It may be recalled that the inertial measuring system provides only velocity and attitude increments from accelerometer and rate-gyro measurements respectively while a GPS receiver estimates the aircraft's position from pseudo-range and carrier phase measurements. On the other hand when the measurement data is provided to a centralised processor where the fusion or mixing of the measurements is done, the system is tightly coupled. Generally, tightly coupled systems are facilitated by centralised

processing while loosely coupled systems are characterised by decentralised or distributed processing. The centralized tightly coupled approach provides the best performance in navigation systems and is generally realised by a single robust Kalman filter. For purposes of fault detection and isolation adequate redundancy is generally provided by replicating the centralised processing in each of the component subsystems.

Vision-based control during the landing phase concerns the problem of using a camera as a sensor in order to identify the aircraft's position relative to the runway based on a real-time visual features state-vector of key landmarks. In practice what one has is measurements of translational accelerations and angular velocity component rates, while visual features of the runway can be extracted from the analysis of an image obtained from a camera. The visual features state-vector is estimated in real-time from images of key landmarks obtained by a camera and measurements of the aircraft's translation and angular velocities.

For landing applications a vital problem is to first recognize the runway and then be able to precisely estimate the runway position relative to the aircraft. Shang and Shi [21] considered the problem of vision-based runway recognition for landing applications. Bourquardez and Chaumette [2] developed algorithms for visual servoing of an airplane requiring alignment with respect to a runway, without explicit estimation. Several authors, Espiau, Chaumette, and Rives [5], Kelly [9], Malis, Chaumette, and Boudet [14], Kelly, Carelli, Nasisi, Kuchen, and Reyes [10], Malis, Chaumette, and Boudet [15], Malis [13], have adopted this strategy for direct visual servoing without explicit estimation. Relatively accurate measurements can be made of the target image; direct visual servoing to align the aircraft along the runway is possible. However solving the runway estimation problem serves a dual purpose of runway recognition as well as position estimation and is therefore highly desirable. Furthermore, the image based measurements can be mixed with satellite and inertial measurements to generate precise position and orientation information for landing control. Shakernia, Ma, Koo and Sastry [20] consider the dual problems of vision based motion estimation and nonlinear landing control.

The algorithm validated in this paper mixes observations of known runway features such as points on the runway boundary or the runway centre-line with inertial and satellite navigation measurements, to provide accurate estimates of both the aircrafts position and orientation during landing. An adaptive unscented Kalman filter based mixing filter is used to integrate kinematic satellite aided inertial navigation system with vision based multiple stereo camera measurements of the same set of five representative points on a runway in a modern receiver that incorporates carrier phase smoothing and ambiguity resolution. Two of the points are assumed to lie

on the runway centreline at the two ends on the runway while the other two are normal to the runway centreline at its mid-point. Using high resolution multiple stereo camera measurements of the five points on the runway, in addition to a set of typical pseudo-range estimates that can be obtained from a satellite navigation system such GPS or GLONASS equipped with a carrier phase receiver, the feasibility of generating high precision estimates of the typical outputs from an inertial navigation system is demonstrated. The methodology may be developed as a stand-alone system or employed in conjunction with a traditional strapped down inertial navigation systems for purposes of initial alignment. Moreover the feasibility of employing adaptive mixing facilitates the possibility of using the system for developing a vision based automatic landing controller.

THE GALILEO SYSTEM
AND NAVIGATION MEASUREMENT'S FEATURES

Europe's Galileo is designed to be a civil system and an independent Global Navigation Satellite System (GNSS). It will consist of a constellation of satellites, complemented by ground stations for system and satellite monitoring as well as control functions, including an integrity function to broadcast real-time warnings of satellite or system malfunctions. The Galileo system architecture also includes a user segment, a space segment, and a ground segment made of a system control and a mission control part. The ESA's first Galileo demonstration satellite Galileo In-Orbit Validation Element (GIOVE-A) was launched in December 2005 and the second (GIOVE-B) was launched successfully in May 2008. The first two satellites of the Galileo system, Galileo FM2 and Galileo PFM, were launched in November, 2011. The Galileo system is expected to be fully operational around 2013. The space segment (Galileo constellation) will consist of 27 satellites, in a 27/3/1 Walker configuration, with a nominal inclination of 56°. The orbit produces seventeen revolutions in approximately ten sidereal days and has a mean semi-major axis of 29600 km. The corresponding orbit period is about 14 hours and 5 minutes and the mean orbit altitude is approximately 23,230 km. Each satellite will broadcast precise ranging and timing signals on several carriers, together with clock synchronization, orbit ephemeris and other data. The satellites are expected to be equipped with both H-Maser clocks (high-stability, satellite primary clocks) and Rubidium (RAFS) clocks (as backup clocks) [3]. The Galileo Signal-in-Space (SIS) data channels transmit four different message types according to the general contents:

— Freely Accessible Navigation message type and related signal (F/Nav);
— Integrity Navigation message type and related signals (I/Nav);

— Commercial Navigation message type and related signal (C/Nav);
— Governmental Access Navigation message type and related signals (G/Nav).

The Galileo navigation services are determined by the data transmitted through the navigation messages, allocated on the E5a, E5b, E6, and E1 sub-carriers. The Galileo navigation signals are transmitted in all four of these frequency bands. The interoperability and compatibility of Galileo and GPS is realized by having two common centre frequencies in E5a/L5 and E1/L1. E5b and E6 straddle the L2 band. Bothe the E5a and E1 bands are wider than the corresponding GPS signal bands, L5 and L1. The Galileo signal in space structure theoretically allows very accurate satellite pseudo-ranging measurements which, in conjunction with the constellation coverage and geometrical capabilities, should meet the Galileo system performance requirements [4, 6]. Following the launch of the first Galileo experimental satellite (GIOVE-A) analysis of real Galileo signals has shown that the Galileo code observables are capable of better positioning performance that the GPS C/A code [16]. Furthermore the basic observation equations for both the code phase and carrier phase measurements are similar for GPS and Galileo, with the process noise covariance in the Galileo signals being generally slightly lower than the corresponding process noise covariance in the GPS signals. It is assumed in this paper that the 27 satellites are located in three planes at 120° to the orbit plane of the primary satellite and in slots at 40° intervals from the primary satellite. The primary satellite is assumed to be either, GIOVE-A, the GIOVE-B or the Galileo FM2 satellite. The orbits of these three satellites are shown in fig. 1. The nearest three satellites visible from a particular latitude and longitude on the Earth's surface are used for pseudo-range simulation.
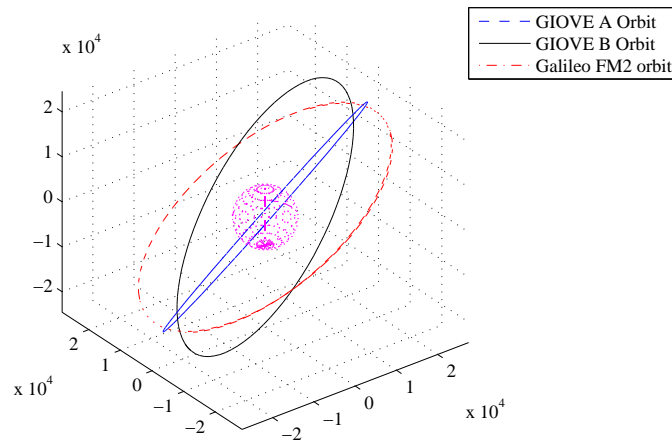

Fig. 1. Orbits of the three Galileo satellites based on position measurements
on 4th November, 2011 [own study]

RUNWAY CO-ORDINATES AND STEREO MEASUREMENTS

Consider a camera fixed to an aircraft and directly viewing a runway. The runway is assumed to be ideally a rectangle and the five points that characterise it are assumed to be the midpoints of the four sides and the geometric centre of the rectangle. Once the runway edge locations are determined the coordinates of these five points can be obtained by successively averaging the coordinates of points along each edge as well as the points on all edges.

The relative position of the camera with reference to the runway is defined in terms of three coordinates as was done by Ho and McClamroch [7]. These are the distance along the line joining from the centre of the camera's lens to the geometric centre point of the runway, R, and two angles (β, ρ) defining the longitudinal orientation of the line with respect to runway centre line and the lateral orientation normal to the runway centre line. If the camera's position relative to the runway could be described in terms of Cartesian (x, y, z), the spherical coordinates (R, β, σ) are related to the Cartesian coordinates by,

$$x = R\cos\beta\cos\sigma \, , \ y = R\cos\beta\sin\sigma \, , \ z = -R\sin\beta \, . \tag{1}$$

Hence, R, β and ρ are obtained from the relations,

$$R\cos\beta = \sqrt{x^2 + y^2} \, , \ \sigma = \sin^{-1}\left(\frac{y}{R\cos\beta}\right), \tag{2}$$

and it follows that,

$$R = \sqrt{x^2 + y^2 + z^2} \, , \ \beta = atan2\left(-\frac{z}{R}, \sqrt{x^2 + y^2}\right), \ \rho = \sin^{-1}(\frac{y}{R}), \tag{3}$$

where *atan2*(.) is the standard MATLAB inverse tangent function for extracting the angle from its sine and cosine components.

The orientation of the camera is defined by three angles (α, γ, δ). α and γ are rotations of the body about the lateral and longitudinal axes respectively and defined in figs. 4a and 4b. The third angle is the rotation about the third axis that is assumed to be mutually perpendicular to the other two. The three angles are related to the 3-2-1 sequence of Euler angles by the relations,

$$\phi = \delta \, , \ \theta = \gamma + \beta \, , \ \psi = \sin^{-1}\left[\frac{\sin(\alpha + \rho)}{\cos(\gamma + \beta)}\right]. \tag{4}$$

The inverse relations are,

$$\alpha = \sin^{-1}\left(\cos\theta\sin\psi\right) - \rho \, , \ \gamma = \theta - \beta \, , \ \delta = \phi \, . \tag{5}$$

Finally the Euler angles are related to the quaternion parameters, which are used for computations to avoid singularities, by,

$$
\begin{bmatrix} q_1 \\ q_2 \\ q_3 \\ q_4 \end{bmatrix} = \begin{bmatrix} \cos\left(\dfrac{\psi}{2}\right)\cos\left(\dfrac{\theta}{2}\right)\sin\left(\dfrac{\phi}{2}\right) - \sin\left(\dfrac{\psi}{2}\right)\sin\left(\dfrac{\theta}{2}\right)\cos\left(\dfrac{\phi}{2}\right) \\ \cos\left(\dfrac{\psi}{2}\right)\sin\left(\dfrac{\theta}{2}\right)\cos\left(\dfrac{\phi}{2}\right) + \sin\left(\dfrac{\psi}{2}\right)\cos\left(\dfrac{\theta}{2}\right)\sin\left(\dfrac{\phi}{2}\right) \\ -\cos\left(\dfrac{\psi}{2}\right)\sin\left(\dfrac{\theta}{2}\right)\sin\left(\dfrac{\phi}{2}\right) + \sin\left(\dfrac{\psi}{2}\right)\cos\left(\dfrac{\theta}{2}\right)\cos\left(\dfrac{\phi}{2}\right) \\ \cos\left(\dfrac{\psi}{2}\right)\cos\left(\dfrac{\theta}{2}\right)\cos\left(\dfrac{\phi}{2}\right) + \sin\left(\dfrac{\psi}{2}\right)\sin\left(\dfrac{\theta}{2}\right)\sin\left(\dfrac{\phi}{2}\right) \end{bmatrix}.
\tag{6}
$$

The Euler angles may be uniquely extracted from a quaternion as:

$$
\sin(\psi)/\cos(\psi) = 2(q_1 q_2 + q_3 q_4)/(q_4^2 + q_1^2 - q_2^2 - q_3^2);
\tag{7a}
$$

$$
\sin(\theta) = -2(q_1 q_3 - q_2 q_4);
\tag{7b}
$$

$$
\sin(\phi)/\cos(\phi) = 2(q_1 q_4 + q_3 q_2)/(q_4^2 - q_1^2 - q_2^2 + q_3^2).
\tag{7c}
$$

In the case of stereo, two cameras take pictures of a same object space but with a different view. The two dimensional images on the plane of projection represent the object in the camera image. These two images contain some encrypted information, the image-depth which is the same for both. This information is the third dimension of two dimensional images. Therefore, the object distance and its depth can be determined by using stereo cameras. With reference to fig. 2 the distance between the two points of view is called the baseline. The end to end baseline's distance affects the range resolution, which in turn influences the range of the depth that can be calculated. The difference in the distance on the image plane of a typical point in the object between its two images is known as the disparity in the images of the point.
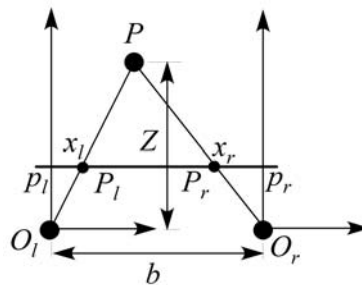

Fig. 2. Geometry of stereo imaging on a common plane for depth estimation [own study]

Typically a stereo system uses a horizontal baseline. The cameras are assumed to be placed at the same elevation. The process of stereo vision is then typically defined as explicitly matching the features in left and right images by finding a transformation relating the two. The stereo baseline b is the distance between the centres of the projection O_l and O_r. The x_l and x_r are the coordinates of P_l and P_r with respect to the principal points p_l and p_r, where the f is a focal length of the camera. The depth of P is estimated by the following equation:

$$\frac{b + x_l - x_r}{Z - f} = \frac{b}{Z}. \qquad (8)$$

Hence it can be shown that in terms of the disparity d,

$$Z = f \frac{Z}{x_r - x_l} = f \frac{b}{d} \text{ and } d = f \frac{b}{Z}. \qquad (9)$$

In a stereo camera, including two views of the same scene is equivalent to adding an additional measurement of the disparity d, for each point measured. Thus stereo camera measurements can be assumed to enhance the observability provided by them as well as increase the number of measurements provided by 50%.

The stereo camera is assumed to provide measurements of the five points characterising the runway. The last of these points is the geometrical centre of the runway which is also the mean of the first four points. Of the first four points, two lie along the runway centre line while the other two are along the line normal to the runway centre-line at its mid-point. Subtracting the runway centre from the coordinates of the four other points, they may be related to the camera coordinates, for the jth camera, by the relations,

$$\overline{X}_{1m,j} = X_{1,j} - x_{c,j} = \frac{fL \cos \rho_j \cos \delta_j}{R_j \cos \alpha_j + L \sin(\rho_j + \alpha_j)} + n_{v1,j}; \qquad (10a)$$

$$\overline{Y}_{1m,j} = Y_{1,j} - y_{c,j} = \frac{fL \cos \rho_j \sin \delta_j}{R_j \cos \alpha_j + L \sin(\rho_j + \alpha_j)} + n_{v2,j}; \qquad (10b)$$

$$\overline{X}_{2m,j} = X_{2,j} - x_{c,j} = \frac{fL \cos \rho_j \cos \delta_j}{R_j \cos \alpha_j - L \sin(\rho_j + \alpha_j)} + n_{v3,j}; \qquad (10c)$$

$$\overline{Y}_{2m,j} = Y_{2,j} - y_{c,j} = \frac{fL \cos \rho_j \sin \delta_j}{R_j \cos \alpha_j - L \sin(\rho_j + \alpha_j)} + n_{v4,j}; \qquad (10d)$$

$$\overline{X}_{3m,j} = X_{3,j} - x_{c,j} = \frac{fW\cos\beta_j\sin\delta_j}{R_j\cos\gamma_j + W\sin(\beta_j+\gamma_j)} + n_{v5,j}; \qquad (10e)$$

$$\overline{Y}_{3m,j} = Y_{3,j} - y_{c,j} = \frac{fW\cos\beta_j\cos\delta_j}{R_j\cos\gamma_j + W\sin(\beta_j+\gamma_j)} + n_{v6,j}; \qquad (10f)$$

$$\overline{X}_{4m,j} = X_{4,j} - x_{c,j} = \frac{fW\cos\beta_j\sin\delta_j}{R_j\cos\gamma_j - W\sin(\beta_j+\gamma_j)} + n_{v7,j}; \qquad (10g)$$

$$\overline{Y}_{4m,j} = Y_{4,j} - y_{c,j} = \frac{fW\cos\beta_j\cos\delta_j}{R_j\cos\gamma_j - W\sin(\beta_j+\gamma_j)} + n_{v8,j}. \qquad (10h)$$

In the equations (10), f is the focal length of the cameras, $2L$ is the length of the runway and $2W$ is the width of the runway and $n_{v1,j}$ to $n_{v8,j}$, are scalar white noise processes of known intensity for the jth camera. In addition, in the case stereo cameras which share a common image plane as shown in Fig. 2, disparity measurements can also be made. These are related to the position of the runway points by the relations,

$$d_{k,j,j+1} = f\frac{b}{Z_{n,k,j,j+1}} + n_{v8+k,j,j+1}, \ k = 1,\ldots 4$$

for each camera pair $(j, \ j-1)$ in a stereo configuration where $Z_{n,k,j,j+1}$ is the normal distance of kth runway point from the camera pair baseline and $n_{v8+k,j,j+1}$ are scalar white noise processes of known intensity for the kth runway point and the jth and $j+1^{\text{th}}$ camera pair. The normal distance of kth runway point from the $(j, \ j-1)$ camera pair's baseline, $Z_{n,k,j,j+1}$ is computed from,

$$Z_{n,k,j,j+1} = \frac{\left|\left(p_{j+1}^c - p_j^c\right)\times\left(p_j^c - p_k^r\right)\right|}{\left|p_{j+1}^c - p_j^c\right|},$$

where p_k^r is the vector position of the runway point in Earth coordinates and p_j^c is the vector position of the jth camera's reference frame origin in Earth coordinates.

PROCESS MODELLING AND GNSS MEASUREMENTS

The complete high precision navigation equations have been derived by [25]. These are summarised here for completeness:

$$
\begin{bmatrix} \dot{V}_N \\ \dot{V}_E \\ \dot{V}_D \end{bmatrix} = \begin{bmatrix} A_N \\ A_E \\ A_D \end{bmatrix} + \begin{bmatrix} 0 \\ 0 \\ g \end{bmatrix} + \begin{bmatrix} -\left(2\omega_s \sin\lambda + \dfrac{V_E}{R_P + h}\tan\lambda\right)V_E + \dfrac{V_N V_D}{R_M + h} \\ \left(2\omega_s \sin\lambda + \dfrac{V_E}{R_P + h}\tan\lambda\right)V_N + \left(2\omega_s \cos\lambda + \dfrac{V_E}{R_P + h}\right)V_D \\ -\dfrac{V_N^2}{R_M + h} - \left(2\omega_s \cos\lambda + \dfrac{V_E}{R_P + h}\right)V_E \end{bmatrix},
$$

$$
\dot{\lambda} = \frac{V_N}{R_M + h}, \quad \dot{\varphi} = \frac{V_E \sec\lambda}{R_P + h}, \quad \dot{h} = -V_D, \tag{11}
$$

where V_N, V_E and V_D are the north, east and down velocities in the local tangent plane, with reference to a local geodetic frame often referred to as the navigation frame (*n*-frame) or north-east-down frame. The last three equations relate these velocities to the rate of change of the geodetic latitude (λ), the rate of change of longitude (φ) and the altitude (h) rate. A_N, A_E and A_D are the north, east, down components of the measured acceleration in the *n*-frame which must be compensated by adding the acceleration due to gravity g, in down direction, ω_s is angular velocity of the Earth, R_M and R_P are the radii of curvature in the meridian and prime vertical at a given latitude. The acceleration components are defined by,

$$
\mathbf{A}_{NED} = \mathbf{D}_{n,b}\left[\mathbf{D}^{-1}(\mathbf{A}_m + \mathbf{b}_1 + \mathbf{n}_1) + \Delta\mathbf{F}\right] \tag{12a}
$$

and

$$
\mathbf{G}_{NED} = \mathbf{D}_{n,b}\left[\mathbf{D}^{-1}\mathbf{G}\right] = \begin{bmatrix} 0 & 0 & g \end{bmatrix}^T, \tag{12b}
$$

where, $\Delta\mathbf{F} \equiv \left([\boldsymbol{\omega}_s \times \boldsymbol{\omega}_s \times \mathbf{r}] - [\boldsymbol{\omega} \times \boldsymbol{\omega} \times \mathbf{r}]\right)$, $\boldsymbol{\omega}_s$ is the Earth's rotation rate vector, $\mathbf{D}_{n,b}$ is the transformation of the measured body acceleration components to the north, east, down components in the navigation or *n*-frame, $\mathbf{G}$ is the gravitational component of the acceleration in the body frame, $\mathbf{A}_m$ is the actual measured acceleration vector obtained from a triad of pendulous accelerometers, $\mathbf{b}_1$ is a measurement bias and drift vector and $\mathbf{n}_1$ is a measurement white noise vector. The matrix $\mathbf{D}$ is defined as,

$$\mathbf{D} = \begin{bmatrix} \mathbf{d}_1^T & \mathbf{d}_2^T & \mathbf{d}_3^T \end{bmatrix}^T,$$

where the vectors $\mathbf{d}_i$ are defined as,

$$\begin{bmatrix} \mathbf{d}_i \end{bmatrix} \equiv \begin{bmatrix} -\mathbf{z}^i \cdot \mathbf{r}_\times^i & \mathbf{z}^i \end{bmatrix} = \begin{bmatrix} z_3^i r_2^i - z_2^i r_3^i & z_1^i r_3^i - z_3^i r_1^i & z_2^i r_1^i - z_1^i r_2^i & z_1^i & z_2^i & z_3^i \end{bmatrix}$$

$$\begin{bmatrix} \mathbf{z}^i \end{bmatrix} = \begin{bmatrix} z_1^i & z_2^i & z_3^i \end{bmatrix}, \tag{13}$$

$\mathbf{z}^i$, is the direction of sensitivity of the ith accelerometer and $\mathbf{r}^i$ is the position vector of the accelerometer location in the body fixed frame. The transformation of the measured body acceleration components to the north, east, down components in the n-frame $\mathbf{D}_{n,b}$, satisfies the differential equation,

$$\dot{\mathbf{D}}_{n,b} + \mathbf{\Omega}_G \mathbf{D}_{n,b} = \mathbf{D}_{n,b} \mathbf{\Omega}_b. \tag{14}$$

In equation (14) the matrix $\mathbf{\Omega}_G$ is obtained from the components of the angular velocity vector of the local geodetic frame or n frame. The angular velocity vector of the local geodetic frame or n frame may be expressed in terms of the Earth angular velocity in the local geodetic frame $\mathbf{\omega}_s$ as,

$$\mathbf{\omega}_G = \mathbf{\omega}_s + \begin{bmatrix} \dot{\varphi}\cos\lambda \\ -\dot{\lambda} \\ -\dot{\varphi}\sin\lambda \end{bmatrix} \text{ with } \mathbf{\omega}_s = \omega_s \begin{bmatrix} \cos\lambda \\ 0 \\ -\sin\lambda \end{bmatrix}. \tag{15}$$

The drift and bias vectors are assumed to be a first order Gauss-Markov processes given by,

$$\dot{\mathbf{b}}_1 = \mathbf{b}_2 + \mathbf{n_2}, \ \dot{\mathbf{b}}_2 = \mathbf{n}_3, \tag{16}$$

where $\mathbf{n}_2$, $\mathbf{n}_3$, are a white noise vector driving the processes.

The body angular velocity vector, $\mathbf{\omega} = \mathbf{\omega}_b$ is assumed to be measured by a triad of fibre optic laser gyros. Thus the measure angular velocity vector is assumed to be related to the body angular vector,

$$\mathbf{L}\mathbf{\omega}_b = \mathbf{\omega}_m + \mathbf{b}_3 + \mathbf{n}_4, \tag{17}$$

where $\mathbf{L}$ is matrix of the three directions of sensitivity of the fibre-optic laser gyros, $\mathbf{\omega}_m$ the actual measured angular velocities, $\mathbf{b}_2$ is a measurement bias and drift vector and $\mathbf{n}_3$ is a measurement white noise vector. Following Savage (1998a) and

Savage (1998b) the bias and drift vector is assumed to be a first order Gauss-Markov process given by,

$$\dot{\mathbf{b}}_3 = \mathbf{b}_4 + \mathbf{n}_5 \ , \ \dot{\mathbf{b}}_4 = \mathbf{n}_6 , \tag{18}$$

where $\mathbf{n}_5$, $\mathbf{n}_6$, are a white noise vector driving the processes.

The attitude quaternion is then computed from the equations,

$$\dot{\mathbf{q}} = \frac{1}{2}\Omega(\omega)\mathbf{q} \ , \ \Omega(\omega) = \begin{bmatrix} 0 & \omega_3 & -\omega_2 & \omega_1 \\ -\omega_3 & 0 & \omega_1 & \omega_2 \\ \omega_2 & -\omega_1 & 0 & \omega_3 \\ -\omega_1 & -\omega_2 & -\omega_3 & 0 \end{bmatrix} , \ \omega = \begin{bmatrix} \omega_1 \\ \omega_2 \\ \omega_3 \end{bmatrix} , \tag{19}$$

where the quaternion components are subject to the constraint $q_1^2 + q_2^2 + q_3^2 + q_4^2 = 1$. Once the solution for the quaternion is known, the transformation from the inertial to the body fixed frame $\mathbf{D}_{b,I}$ is computed from,

$$\mathbf{D}_{b,I}(\mathbf{q}) = \begin{bmatrix} q_4^2 + q_1^2 - q_2^2 - q_3^2 & 2(q_1 q_2 + q_3 q_4) & 2(q_1 q_3 - q_2 q_4) \\ 2(q_1 q_2 - q_3 q_4) & q_4^2 - q_1^2 + q_2^2 - q_3^2 & 2(q_2 q_3 + q_1 q_4) \\ 2(q_1 q_3 + q_2 q_4) & 2(q_2 q_3 - q_1 q_4) & q_4^2 - q_1^2 - q_2^2 + q_3^2 \end{bmatrix} . \tag{20}$$

and its inverse is obtained from the same equation by changing the sign of q_4. The required transformation $\mathbf{D}_{n,b}$ may then be computed without matrix inversion from $\mathbf{D}_{n,I}\mathbf{D}_{b,I}^{-1}$, the transformations from the inertial to the *n*-frame and the inverse transformation from the inertial to the body fixed frame. Alternately $\mathbf{D}_{n,b}$ may be computed directly from the associated quaternion, representing the relative attitude of the navigation from relative to the body frame. The vision based measurements of the four pairs of coordinates of points on the runway relative to the runway centre are assumed to be functions of the body orientation as discussed in the previous section.

The actual pseudo-range vector is related to the geodetic latitude λ, geocentric latitude λ_s, longitude ϕ and altitude *h*, by the relations,

$$\rho = \begin{bmatrix} r_s \cos\lambda_s \cos\phi + h\cos\lambda\cos\phi \\ r_s \cos\lambda_s \sin\phi + h\cos\lambda\sin\phi \\ r_s \sin\lambda_s + h\sin\lambda \end{bmatrix} \tag{21}$$

where $\boldsymbol{\rho}$ is the Earth centred, Earth fixed position vector of the aircraft, r_s the radius at a surface point of the flattened Earth ellipsoid and λ_s are defined in terms of the flattening f and the equatorial radius R_e as,

$$\lambda_s = \arctan\!\left((1-f)^2 \tan\lambda\right) \tag{22}$$

and

$$r_s = \sqrt{R_e^2 \Big/ \left(1 + \left(1\big/(1-f)^2 - 1\right)\sin^2\lambda_s\right)}. \tag{23}$$

The Galileo pseudo range measurement model and the model of the Hatch filter for mixing the corresponding code based measurements with carrier phase measurements are implemented in discrete form as discussed by [25].

ADAPTIVE UNSCENTED KALMAN FILTERING

The mixing filter is implemented as an adaptive unscented Kalman filter. The basic unscented Kalman filter is identical to the filter implemented in [25].

Consider a random variable $\mathbf{w}$ with dimension L which is going through the nonlinear transformation, $\mathbf{y} = \mathbf{f}(\mathbf{w})$. The initial conditions are that $\mathbf{w}$ has a mean $\overline{\mathbf{w}}$ and a covariance $\mathbf{P}_{ww}$. To calculate the statistics of $\mathbf{y}$, a matrix χ of $2L + 1$ sigma vectors is formed. We have chosen to use the scaled unscented transformation proposed by Julier [8], as this transformation gives one the added flexibility of scaling the sigma points to ensure that the covariance matrices are always positive definite.

Given a general discrete nonlinear dynamic system in the form,

$$\mathbf{x}_{k+1} = \mathbf{f}_k\!\left(\mathbf{x}_k, \mathbf{u}_k\right) + \mathbf{w}_k, \ \ \mathbf{y}_k = \mathbf{h}_k\!\left(\mathbf{x}_k\right) + \mathbf{v}_k, \tag{24}$$

where $\mathbf{x}_k \in R^n$ is the state vector, $\mathbf{u}_k \in R^r$ is the known input vector, $\mathbf{y}_k \in R^m$ is the output vector at time k $\mathbf{w}_k$ and $\mathbf{v}_k$ are, respectively, the disturbance or process noise and sensor noise vectors, which are assumed to Gaussian white noise with zero mean. Furthermore $\mathbf{Q}_k$ and $\mathbf{R}_k$ are assumed to be the covariance matrices of the process noise sequence, $\mathbf{w_k}$ and the measurement noise sequence, $\mathbf{v_k}$ respectively. The unscented transformations of the states are denoted as,

$$\mathbf{f}_k^{UT} = \mathbf{f}_k^{UT}\!\left(\mathbf{x}_k, \mathbf{u}_k\right), \ \mathbf{h}_k^{UT} = \mathbf{h}_k^{UT}\!\left(\mathbf{x}_k\right), \tag{25}$$

while the transformed covariance matrices and cross-covariance are respectively denoted as,

$$\mathbf{P}_k^{ff} = \mathbf{P}_k^{ff}\left(\hat{\mathbf{x}}_k, \mathbf{u}_k\right),\ \mathbf{P}_k^{hh-} = \mathbf{P}_k^{hh}\left(\hat{\mathbf{x}}_k^-\right) \tag{26a}$$

and

$$\mathbf{P}_k^{xh-} = \mathbf{P}_k^{xh-}\left(\hat{\mathbf{x}}_k^-, \mathbf{u}_k\right). \tag{26b}$$

The UKF estimator can then be expressed in a compact form. The state time-update equation, the propagated covariance, the Kalman gain, the state estimate and the updated covariance are respectively given by,

$$\hat{\mathbf{x}}_k^- = \mathbf{f}_{k-1}^{UT}\left(\hat{\mathbf{x}}_{k-1}\right); \tag{27a}$$

$$\hat{\mathbf{P}}_k^- = \mathbf{P}_{k-1}^{ff} + \mathbf{Q}_{k-1}; \tag{27b}$$

$$\mathbf{K}_k = \hat{\mathbf{P}}_k^{xh-}\left(\hat{\mathbf{P}}_k^{hh-} + \mathbf{R}_k\right)^{-1}; \tag{27c}$$

$$\hat{\mathbf{x}}_k = \hat{\mathbf{x}}_k^- + \mathbf{K}_k\left[\mathbf{z}_k - \mathbf{h}_k^{UT}\left(\hat{\mathbf{x}}_k^-\right)\right]; \tag{27d}$$

$$\hat{\mathbf{P}}_k = \hat{\mathbf{P}}_k^- - \mathbf{K}_k\left(\hat{\mathbf{P}}_k^{hh-} + \mathbf{R}_k\right)^{-1}\mathbf{K}_k^T. \tag{27e}$$

Equations (27) are in the same form as the traditional Kalman filter and the extended Kalman filter. Thus higher order non-linear models capturing significant aspects of the dynamics may be employed to ensure that the Kalman filter algorithm can be implemented to effectively estimate the states in practice.

In order to employ the UKF when precise statistics of the process and measurement noise vectors are not available, the adaptive filter method proposed by Song, Qi and Han [23] is used to estimate the orbit parameters. The covariance matrixes of measurement residuals are recursively updated in the UKF. The measurement noise covariance matrices, in the case of the UKF, may be expressed as:

$$\hat{\mathbf{R}}_k = \mathbf{C}_r^{k,N} + \hat{\mathbf{P}}_k^{hh}, \tag{28}$$

where, $\mathbf{C}_r^{k,N}$ is defined in terms of the sample size N and the residual $\mathbf{r}_k$ as,

$$\mathbf{C}_r^{k,N} = \frac{1}{N}\sum_{j=k-N+1}^{k}\mathbf{r}_j\mathbf{r}_j^T,\ \mathbf{r}_k = \left(\mathbf{z}_k - \mathbf{H}_k\hat{\mathbf{x}}_k\right) = \mathbf{v}_k + \mathbf{H}_k\left(\mathbf{x}_k - \hat{\mathbf{x}}_k\right). \tag{29}$$

Equation (28) involves the further computation of $\hat{\mathbf{P}}_k^{hh}$, by applying the unscented nonlinear transformation, $\mathbf{h}_k^{UT}\left(\hat{\mathbf{x}}_k\right)$ to the state estimate, $\hat{\mathbf{x}}_k$. The measurement

noise covariance may be updated in principle by employing the equation (28). The nonlinear relationships between the covariance matrices also suggests that the update of $\mathbf{R}_k$ could be done by employing the covariance of the residual.

In the application considered in this paper, the adaptation of $\mathbf{Q}_k$ is implemented, as it is the process statistics that is often unknown or may be considered to vary. It was observed that the magnitudes of the filter gains were relatively small and for these reasons the exact expression for an estimate of $\mathbf{Q}_k$,

$$\hat{\mathbf{Q}}_{k-1} \equiv \mathbf{C}_{\Delta x}^{k,N} + \hat{\mathbf{P}}_k - \mathbf{P}_{k-1}^{ff} \tag{30a}$$

was approximated as,

$$\hat{\mathbf{Q}}_{k-1} \approx \mathbf{C}_{\Delta x}^{k,N}, \tag{30b}$$

where $\mathbf{C}_{\Delta x}^{k,N}$ is defined as,

$$\mathbf{C}_{\Delta x}^{k,N} = \frac{1}{N} \sum_{j=k-N+1}^{k} \Delta \mathbf{x} \Delta \mathbf{x}^T \approx \hat{\mathbf{P}}_k^- - \hat{\mathbf{P}}_k = \mathbf{K}_k \mathbf{H}_k \hat{\mathbf{P}}_k^= \tag{31}$$

and

$$\Delta \mathbf{x} = \left(\mathbf{x}_k - \hat{\mathbf{x}}_k^- \right) - \left(\mathbf{x}_k - \hat{\mathbf{x}}_k \right). \tag{32}$$

VISION-GNSS-INS
INTEGRATED MIXING FILTER MECHANISATION

The process model for applying the adaptive UKF is exactly the same as in [25]. The primary difference is that the method of measurement of the attitude by using multiple antennas adopted in [25] is now replaced by the camera based measurements of the four pre-selected points on the runway.

To test the filter performance and to subject it to realistic accelerations over an extended period of time, the aircraft was assumed to descending in the vicinity of London Heathrow. The initial altitude of the vehicle was assumed to be 10 000 metres while the initial location was assumed to be approaching London Heathrow. The simulations were compared with the both the adaptive and non-adaptive (standard) UKF. The comparison is made over a typical epoch of 30 seconds (= 15×10^4 time steps) and compared with the corresponding simulations. The time step for implementing the estimator was chosen as, $\Delta t = 0.0005$ seconds. In figures 3, 4, 5, 6 and 7 the results obtained using the UKF without adaptation are compared with the simulations. Only the responses over the last 12 seconds are shown in the figures. From the figures 3–7 it is observed that the aircraft was subjected to a relatively large random disturbance after about 10 seconds.
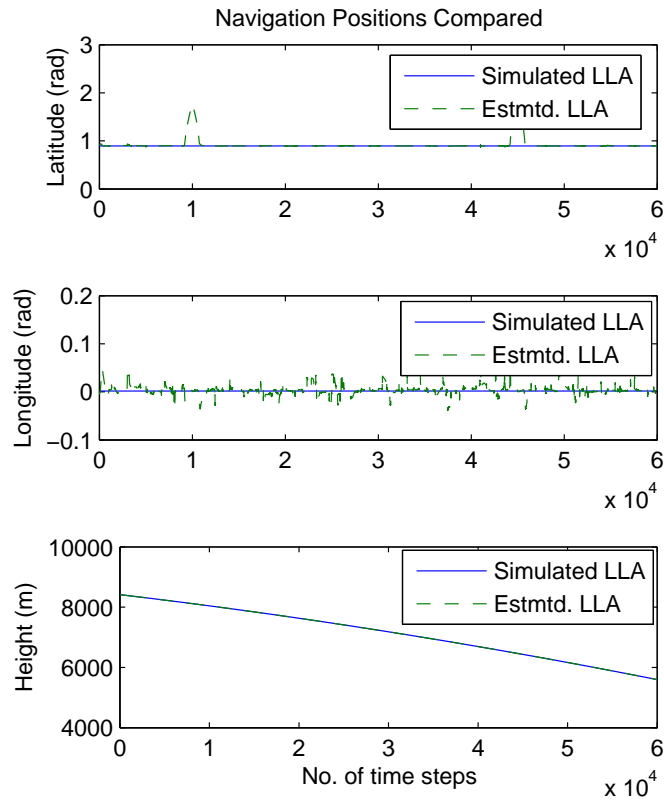
Fig. 3. Comparison of the UKF estimates and simulations of the latitude (rad), longitude (rad) and attitude in metres (LLA) [own study]
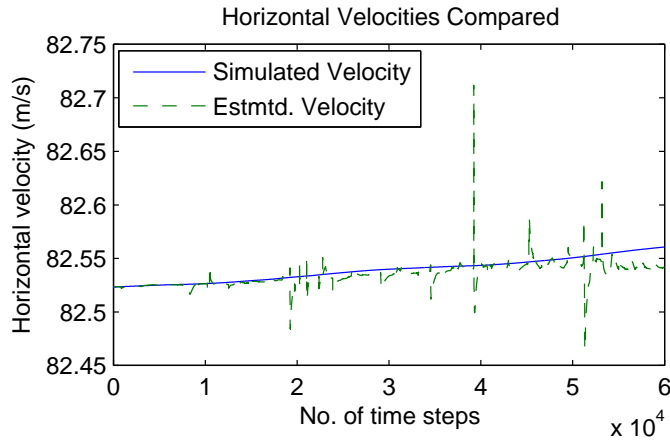

Fig. 4. Comparison of the UKF estimates and simulations of the aircraft's horizontal velocity [own study]
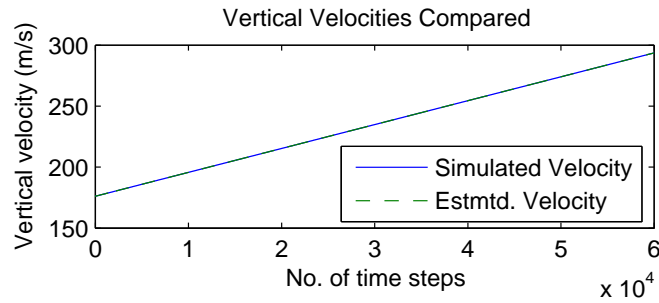
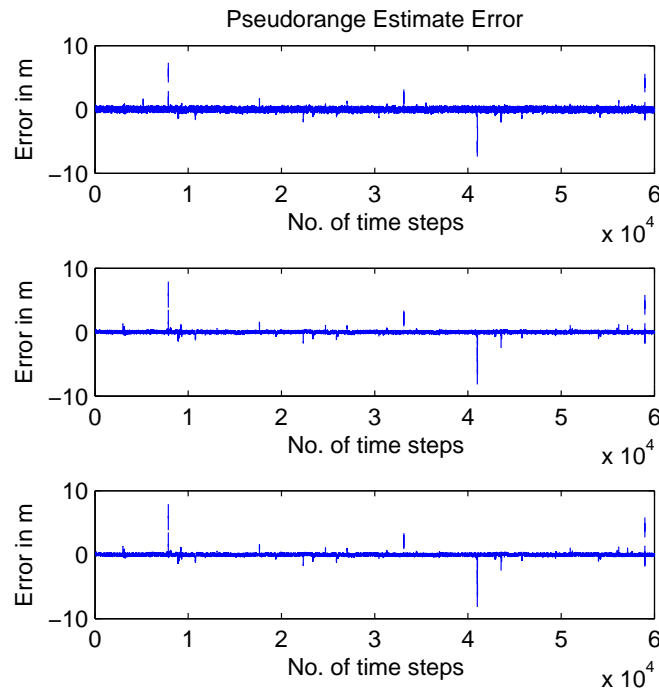Fig. 5. Comparison of the UKF estimates and simulations of the aircraft's vertical velocity
[own study]

Fig. 6. Estimates of the Pseudo-range error components obtained
by the non-adaptive (standard) UKF for an INS-GNSS (GALILEO) system [own study]

It is observed from fig. 6 and 7 that when the vision measurements were mixed with the simulated INS-GNSS (GALILEO) measurements, the predicted pseudo-range errors are comparable to the corresponding errors obtained by mixing with INS-GPS measurements. However the errors were generally noisier, with the noise magnitudes about the same as the perturbations due to attitude changes, thus making it impossible to

predict the attitude quaternion components accurately. It is also interesting to observe that the estimator recovered with respect to all the states and it continues to track the measurements after recovering from the effects of the disturbance. In the case of the adaptive UKF, the estimator was able to perform as well as the non-adaptive case only in the case of position estimates. This is illustrated in figure 8. In the case of orientation or attitude estimates, both the standard and adaptive UKF were unable to accurately estimate the quaternion components for INS-GNSS (GALILEO) simulated measurements. This was due to the lack of accurate orbit data for an adequate number of independent GALILEO satellites. While the methodology worked well with simulated INS-GPS measurements, it was unable to accurately estimate the quaternion components with the three available GALILEO satellite measurements.
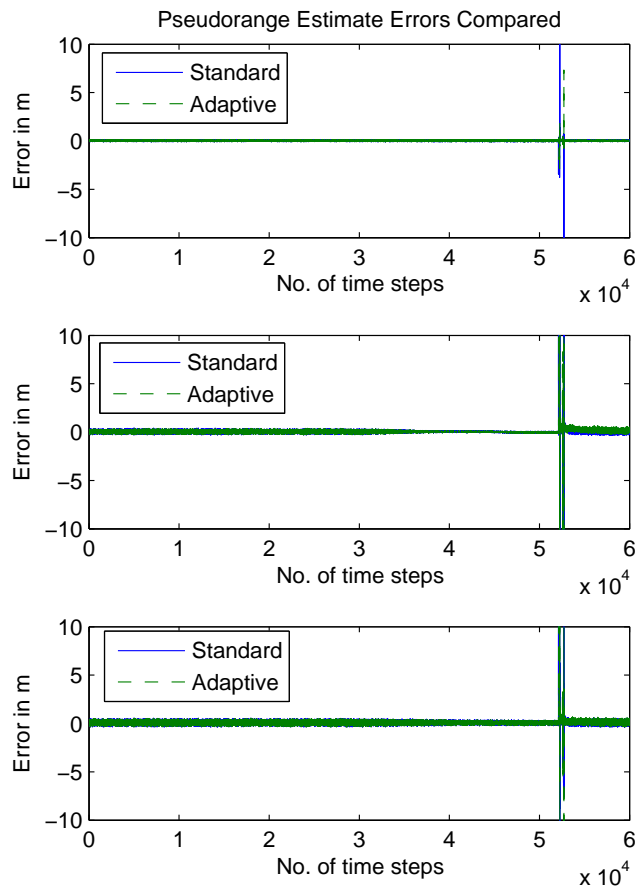

Fig. 7. Comparison of the adaptive and non-adaptive (standard) UKF pseudo-range estimate error components for an INS-GPS system [own study]
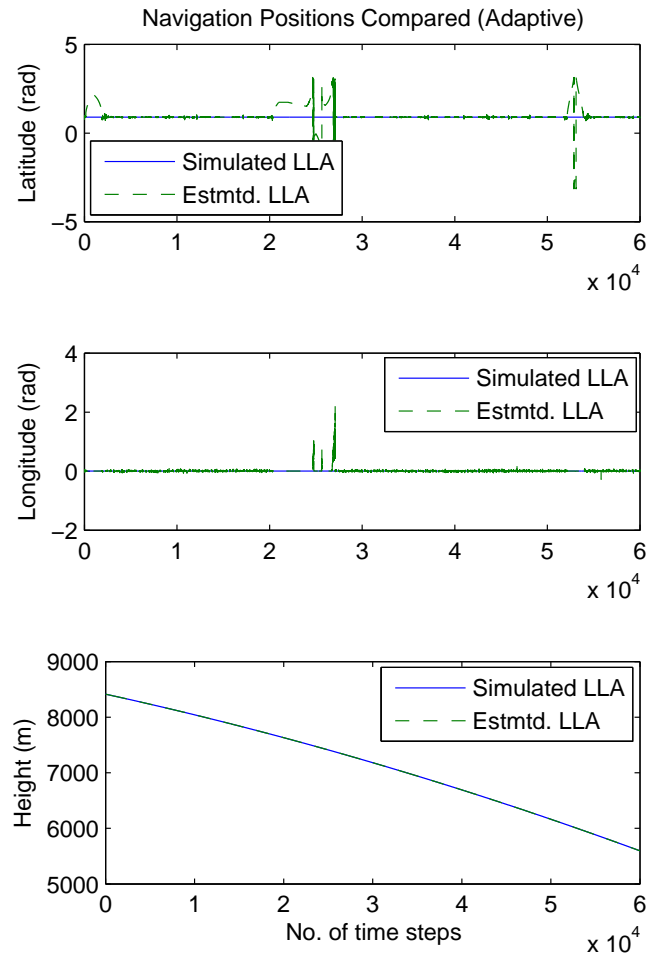
Fig. 8. Comparison of the adaptive UKF estimates and simulations of the latitude (rad),
longitude (rad) and attitude in metres (LLA) [own study]

CONCLUSIONS

In this paper we have successfully demonstrated the integration of camera measurements of five representative points on a runway with a GNSS-INS (GALILEO) navigation system to successfully predict the position and orientation of an aircraft while it is approaching the runway. In this implementation increasing the number of camera measurements did not increase the accuracy of attitude predictions. On the other hand when the five points on the runway are equidistant from the runway centre the attitude prediction error reduces considerably.

Vision based methods which seek to integrate camera measurements with traditional Satellite Navigation-INS position and orientation estimation have the primary advantage of increasing estimation accuracy as the aircraft approaches the runway. However the methodology is feasible only when the runway is within the field of view of the camera. When the aircraft is relatively far from the runway it is possible in principle to use the horizon measurements or some other known visual or infrared landmark selected from a catalogue of such reference marker points to initialize the estimation. On the other hand as the aircraft approaches closer to landing when the entire runway may not be within the field of view of the camera, an alternate set of five points in the vicinity of the touchdown region could be used to improve the accuracy of position and orientation estimation. The inclusion of such catalogued landmarks to improve the position and orientation estimation accuracy is currently being investigated and will be reported elsewhere.

The ultimate accuracy of the integrated estimation system depends primarily on the characteristics of the image processing in general and methods used to extract the geometrical features from the image in particular which in turn would depend on the pixel quantization of the image plane and computer power available. Yet the results obtained in the paper demonstrate the practical feasibility of the proposed integrated position and orientation estimation system.

REFERENCES

[1] Andrade-Cetto J., Sanfeliu A., The effects of partial observability in SLAM, Proc. of the 2004 IEEE International Conference on Robotics and Automation, pp. 397–402, New Orleans, LA, 2004.

[2] Bourquardez O., Chaumette F., Visual Servoing of an Airplane for Alignment with respect to a Runway, IEEE Int. Conf. on Robotics and Automation, ICRA 2007, pp. 1330–1335.

[3] Dellago R., Detoma E., Spazio A., Galileo-GPS Interoperability and Compatibility: A Synergetic Viewpoint, Proceedings of the ION GPS, 2003.

[4] Dellago R., Pieplu J. M., Stalford R., The Galileo System Architecture at the End of the Design Phase, ION GPS/GNSS, September 2003.

[5] Espiau B., Chaumette F., Rives P., A New Approach to Visual Servoing in Robotics, IEEE Transactions on Robotics and Automation, 1992, Vol. 8, No. 3, pp. 313–325.

[6] Guenter W., Hein J. et al., Status of Galileo Frequency and Signal Design, Proc. of ION GPS, 2002.

[7] Ho C-C. J., McClamroch N. H., Automatic Spacecraft Docking Using Computer Vision-Based Guidance and Control Techniques, Journal of Guidance, Control, and Dynamics, 1993, Vol. 16, No. 2, pp. 281–288.

[8] Julier S. J., The Scaled Unscented Transformation, Proceedings of the American Control Conference, 2002, Vol. 6, pp. 4555–4559.

[9] Kelly R., Robust asymptotically stable visual servoing of planar robots, IEEE Trans. on Robotics and Automation, 1996, Vol. 12, No. 5, pp. 759–766.

[10] Kelly R., Carelli R., Nasisi O., Kuchen B., Reyes F., Stable Visual Servoing of Camera-in-Hand Robotic Systems, IEEE/ASME Transactions on Mechatronics, 2000, Vol. 5, No. 1.

[11] Kim J., Sukkarieh S., Autonomous airborne navigation in unknown terrain environments, IEEE Transactions on Aerospace and Electronic Systems, 2004, 40(3), pp. 1031–1045.

[12] Langelaan J. W., State Estimation for Autonomous Flight in Cluttered Environments, PhD thesis, Stanford University, Department of Aeronautics and Astronautics, 2006,

[13] Malis E., Vision-based control invariant to camera intrinsic parameters: stability analysis and path tracking, IEEE International Conference on Robotics and Automation, Washington, D.C., USA, 2002.

[14] Malis E., Chaumette F., Boudet, S., 2 1/2 d visual servoing, IEEE Trans. on Robotics and Automation, 1999, Vol. 15, No. 2, pp. 234–246.

[15] Malis E., Chaumette F., Boudet S., 2 1/2 d visual servoing with respect to unknown objects through a new estimation scheme of camera displacement, International Journal of Computer Vision, 2000, Vol. 37, No. 1, pp. 79–97.

[16] Navarro-Reyes D., Galileo Programme Status and ongoing GIOVE Experimentation, European Geosciences Union (EGU), Vienna, Austria, 2007.

[17] Roumeliotis S., Johnson A., Montgomery J., Augmenting inertial navigation with image-based motion estimation, IEEE International Conference on Robotics and Automation (ICRA), p. 4326–33, Washington, D.C., USA, 2002.

[18] Savage P., Strapdown inertial navigation integration algorithm design, part 1, Attitude algorithms, Journal of Guidance, Control and Dynamics, 1998, Vol. 21, No. 1, pp. 19–28.

[19] Savage P., Strapdown inertial navigation integration algorithm design, part 2: Velocity and position algorithms, Journal of Guidance, Control and Dynamics, 1998, Vol. 21, No. 3, pp. 208–221.

[20] Shakernia O., Ma Y., Koo T. J., Sastry S., Landing an Unmanned Air Vehicle: Vision Based Motion Estimation and Nonlinear Control, Asian Journal of Control, 1999, Vol. 1, No. 3, pp. 128–145.

[21] Shang J., Shi Z., Vision-based Runway Recognition for UAV Autonomous Landing, IJCSNS International Journal of Computer Science and Network Security, 2007, Vol. 7, No. 3, pp. 112–117.

[22] Sharp C. S., Shakernia O., Sastry S. S., A Vision System for Landing an Unmanned Aerial Vehicle, Proceedings of the IEEE, 2001.

[23] Song Q., Qi J., Han J., An Adaptive UKF Algorithm and Its Application in Mobile Robot Control, ROBIO '06, IEEE International Conference on Robotics and Biomimetics, Kunming, China, 2006, pp. 1117–1122.

[24] Strelow D., Motion estimation from image and inertial measurements, PhD thesis, Carnegie Mellon University, 2004.

[25] Vepa R., Zhahir A., High-Precision Kinematic Satellite and Doppler Aided Inertial Navigation System, The Journal of Navigation, 2011, Vol. 64, No. 1, pp. 91–108.

[26] Wu A., Johnson E., Proctor A., Vision-aided inertial navigation for flight control, Proceedings of the AIAA Guidance, Navigation, and Control Conference, number AIAA 2005–5998, San Francisco, CA, 2005.